Journal of Hazardous Materials 489 (2025) 137607

Contents lists available at ScienceDirect

Journal of Hazardous Materials

journal homepage: www.elsevier.com/locate/jhazmat

Carbon quantum dots as efficient cocatalysts in Fenton-like processes: Preparation optimization and mechanistic insights

Yangfan Xia [a], Xu Huang [b], Kaiqiang Wu [a], Yechao Tian [b], Yifan Shen [b], Jifa Zhang [a], Yongjie Chen [a], Dawei Li [a,*], Feihu Li [a]

[a] Collaborative Innovation Center of Atmospheric Environment and Equipment Technology, Jiangsu Key Laboratory of Atmospheric Environment Monitoring and Pollution Control, School of Environmental Science and Engineering, Nanjing University of Information Science and Technology, 219 Ningliu Road, Nanjing 210044, China

[b] State Key Laboratory of Pollution Control and Resource Reuse, School of the Environment, Nanjing University, Nanjing 210023, China

HIGHLIGHTS

- Electrochemical exfoliation was used to prepare CQDs.
- Preparations can precisely control the carboxyl concentration on CQD surfaces.
- The CQDs-Fe^{3+}/H_2O_2 system shows improved cocatalysis for phenols.
- A linear correlation is established between the carboxyl content and the k_{obs}.

GRAPHICAL ABSTRACT

ARTICLE INFO

Keywords:
Fenton-like catalysis
Electrochemical preparation
Functional group regulation
DFT calculation

ABSTRACT

Carbon quantum dots (CQDs) are promising cocatalysts in Fenton-like technologies, leveraging hydrogen peroxide and boosting Fe^{2+} generation and thereby expediting the advanced oxidation process. Although several studies have shown that the preparation affects the cocatalytic performance of the resulting CQDs, the precise correlation between the preparation and the cocatalytic efficiency is unclear. Here, we combine the batch experiments with the theoretical calculations to systematically explore how the parameters in electrochemical exfoliation preparation affect the cocatalytic performance of the as-prepared CQDs. The results show that adjusting parameters like voltage, electrolyte concentration, and electrolysis duration can precisely regulate the surface functional groups of CQDs, which in turn affects the cocatalytic performance. A linear positive correlation is identified between the surface carboxyl content and the pseudo-first-order rate constant (k_{obs}) in Fenton-like reactions, with the highest carboxyl content (18.26 mmol/g) found in C@C3–30V-24H that induces the optimum catalytic performance to the C@C3–30V-24H-Fe^{3+}/H_2O_2 system for phenol removal (97.75 % versus 21.17 % in Fe^{3+}/H_2O_2 system at pH 3). DFT calculations reveal that phenolic compounds with electron-donating groups are more readily oxidized and that those with lower LUMO levels demonstrate higher k_{obs}. This study underscores the crucial role of CQDs preparation on their cocatalytic performance in Fenton-like reactions.

* Corresponding author.
E-mail address: daweili@nuist.edu.cn (D. Li).

https://doi.org/10.1016/j.jhazmat.2025.137607
Received 1 November 2024; Received in revised form 8 December 2024; Accepted 11 February 2025

1. Introduction

The water crisis due to pollution has gradually escalated into a severe global environmental issue in the context of global climate changes [31]. In particular, industrial wastewater from sectors such as petrochemical, pharmaceutical, and paper manufacturing contains significant levels of phenolic pollutants, including phenol, hydroquinone, and p-nitrophenol. These phenolic pollutants pose substantial threats to both the environment and public health due to their high toxicity, structural stability, and resistance to degradation, making their control a priority in water pollution management [25,53,58]. Traditional biochemical and physical methods like adsorption [20], coagulation-precipitation [64], and membrane separation [43] are feasible in some scenarios but often suffer from inefficient removing high concentrations of phenolic pollutants. As efficient advanced oxidation processes, Fenton and Fenton-like technologies have gained extensive attention in the field of wastewater treatment due to their superior cleanup capabilities, low operational costs, and environmental friendliness [57].

The Fenton reaction can generate hydroxyl radicals (•OH) through the reaction of $Fe^{2+}$and H_2O_2, which is featured by a high redox potential (2.7 V) and can decompose organic pollutants rapidly [4]. The practical application of the Fenton reaction, however, usually has several limitations, such as low utilization rate of hydrogen peroxide, slow reduction rate of Fe^{3+} to Fe^{2+}, loss of iron ions, and formation of iron sludge [5,32]. To address these issues, cocatalysts like semiconductors [16], metal-organic frameworks (MOFs) [52], carbon nanotubes [24], and metal sulfides [59] have been applied effectively. These cocatalysts can enhance Fenton and Fenton-like reactions by improving electron transfer efficiency or providing additional active sites. Additionally, coupled systems such as photo-Fenton [8], electro-Fenton [9], and microwave-Fenton [48] have also been introduced to further boost reaction efficiency. Nonetheless, these methods may encounter issues such as the leaching and loss of active metals, low mass transfer efficiency, and high operation costs [13,28,39].

Carbon quantum dots (CQDs) are emerging zero-dimensional carbon-based nanomaterials, consisting of carbon cores of a few nanometers in size and shells decorated with functional groups, e.g., carbonyl and carboxyl [23,50]. Due to their excellent hydrophilicity, high oxygen content, and favorable electron transfer properties, CQDs are widely used as bioimaging agents [29], light-emitting diodes [51], and photovoltaic devices [7]. Recently, CQDs have been introduced as cocatalysts in Fenton-like reactions, showing promising potential due to their low toxicity, ease of surface functionalization, and lower cost compared to traditional cocatalysts [55,56,61]. Of various preparation methods for CQDs, electrochemical exfoliation represents a "top-down" approach and is simple and high-yielding for synthesizing CQDs. For instance, [65]) successfully synthesized CQDs in an electrolyte (pH = 5) at a cell voltage of 30 V by using two high-purity graphite rods as anodes and cathodes, respectively. More recently, Li et al. [35] have explored the effectiveness of hydroxyl radicals (•OH) that were generated on the cathode surface during the electrolysis of H_2O_2, to facilitate the exfoliation of graphite rods. By using a cell voltage of 30 V for 48 h in an electrolyte solution containing 5 mmol/L H_2O_2, they successfully synthesized carboxyl-functionalized carbon quantum dots (CQD@5) with a carboxyl content of 22.66 mmol/g, which has demonstrated the optimum cocatalytic performance in Fenton-like reactions.

Given the exceptional performance of CQDs in Fenton-like reactions, it would be promising to further optimize the microstructure of CQDs by regulating the preparation parameters, such as cell voltage, electrolyte concentration, and electrolysis time. These parameters not only directly influence the preparation efficiency of CQDs but also significantly regulate their size distribution, morphological characteristics, and the types and quantities of surface oxygen-containing functional groups [47]. To date, although several studies have shown that the preparation affects the cocatalytic performance of the resulting CQDs [35,47], the precise correlation between the preparation and the cocatalytic efficiency is poorly understood.

To this end, this study aims to explore the correlation between the preparation of electrochemical exfoliation and the cocatalytic performance of the as-synthesized CQDs in Fenton-like reactions of phenolic pollutant decomposition. The yield, morphology, and carboxyl content of the CQDs were precisely controlled by adjusting variables such as voltage, electrolyte concentration, and electrolysis duration. Comprehensive analyses using TEM, XPS, and Zeta potential characterization were conducted. The synthesized CQDs were then evaluated as cocatalysts in the Fe^{3+}/H_2O_2 system for degradation of phenol over the pH range of 3 − 8. Additionally, the impact of Fe^{3+}, CQDs, and H_2O_2 on phenol degradation was explored, alongside the reusability and versatility of CQDs within the reaction matrix. Besides, electron paramagnetic resonance (EPR) and radical scavenging experiments were performed to identify the active species responsible for pollutant removal. DFT calculations were employed to analyze the relationship between pollutant degradation performance and their properties. This research not only optimized CQDs preparation but also broadened their application potential in Fenton-like systems, offering a promising approach for water purification.

2. Materials and methods

2.1. Materials

Graphite rods (99.99 %) were purchased from Beijing Jinglong Special Carbon Technology Co., Ltd. Ferric chloride hexahydrate ($FeCl_3 \cdot 6\ H_2O$), hydrogen peroxide (H_2O_2, 30 %), hydroquinone (P-OH), phenol (P), bisphenol A (BPA), para-chlorophenol (P-Cl), para-hydroxybenzaldehyde (P-CHO), para-nitrophenol (P-NO_2), tertbutyl alcohol (TBA), 2,2,6,6-tetramethyl-4-piperidinyloxy (TEMPOL), furfuryl alcohol (FFA) , dimethyl sulfoxide (DMSO) , 2,2,6,6-Tetramethyl-1-piperidinyloxy (TEMP), 5,5-Dimethyl-1-pyrroline N-oxide (DMPO) and 1,10-phenanthroline of analytical grade or higher purity were purchased from Sigma-Aldrich. Hydrochloric acid (HCl, 37.0 %), sulfuric acid (H_2SO_4, >98.0 %), sodium hydroxide (NaOH, ≥96.0 %), and other reagents were purchased from Sinopharm Chemical Reagent Co., Ltd. HPLC-grade methanol (MeOH) was purchased from Merck (Germany). All chemicals were of analytical grade and used without further purification. All stock solutions were prepared using ultrapure water (18.25 MΩ·cm).

2.2. Preparation of CQDs

CQDs were prepared via an electrochemical exfoliation method, by using two commercially available graphite rods as electrodes (electrode spacing = 6 cm) that were inserted into 500 mL of an electrolyte solution with varying concentrations (1, 3, 5 mmol/L) of HCl. Various voltages (20, 30, 40 V) were applied using a DC power supply, while continuous stirring was maintained with a magnetic stirrer throughout the reaction. With increasing electrolysis time (18, 24, 30 h), the anode graphite rods became corroded, leading to a color change from colorless to deep yellow, and eventually to dark brown over time. The resultant solution was filtered using a 0.22 μm membrane and subsequently centrifuged at 8000 rpm for 40 minutes to remove large graphite particles. The solution was then dialyzed in an MW300 dialysis bag over 48 hours to remove the residual Cl^- and $HClO/ClO^-$, yielding to a high-purity CQDs solution [60]. The CQDs samples were labeled as C@CX-YV-ZH based on electrolyte concentrations (X: 1, 3, 5 mmol/L), applied voltages (Y: 20, 30, 40 V), and electrolysis durations (Z: 18, 24, 30 h).

2.3. Characterization of CQDs

Transmission electron microscopy (TEM, JEM2800F, JEOL, Japan) was employed to characterize the morphology and size of the samples at an accelerating voltage of 200 kV. The crystallinity of the samples was

analyzed using X-ray diffraction (XRD, USA) with a Cu Kα radiation source (λ=1.5406 Å) over a range of 2θ= 10–80°. UV–vis absorption spectroscopy was conducted using an Agilent 8453. Raman spectra were recorded on a Horiba Lab RAM HR Evolution Raman spectrometer (Japan). The elemental composition of the samples was analyzed by X-ray photoelectron spectroscopy (XPS) using an AXIS SUPRA+ (Shimadzu, Japan). The surface functional groups of the samples were analyzed using Fourier transform infrared spectroscopy (FTIR, NEXUS 870, NICOLET, USA). The zeta potential of the samples was measured with a Malvern Zetasizer Nano-ZS90 analyzer (UK). EPR experiments were conducted using a Magnettech ESR5000 JEOL (Bruker, Germany).

2.4. Fenton-like degradation experiments

CQDs and Fe^{3+} solutions were added to solutions containing various pollutants, including phenol, hydroquinone, o-nitrophenol, o-aminophenol, and o-methylphenol (10 mg/L). The pH value of the mixture was adjusted to 3 using a 0.1 mol/L solution of H_2SO_4 and NaOH. The pH impact experiments were performed over 3–8. The degradation experiments were conducted under vigorous magnetic stirring conditions. At predetermined time intervals, 1 mL of the solution was sampled using a pipette, filtered through a polytetrafluoroethylene (PTFE) syringe filter (0.22 μm), and then 0.1 mL of methanol was added to quench the reaction. The concentrations of phenol, hydroquinone, o-nitrophenol, o-aminophenol, and o-methylphenol in the samples were then determined. All experiments were conducted in triplicate.

2.5. Analytical methods

The concentration of CQDs was quantified using the drying and weighing method. The content of oxygen-containing functional groups over the CQD surface was determined using the Boehm titration method [65]. The consumption of H_2O_2 was quantified using $TiOSO_4/H_2SO_4$ reagent. The utilization efficiency (η) of H_2O_2 is defined as the ratio of theoretical H_2O_2 consumption ($[\Delta H_2O_2]_S$) to actual hydrogen peroxide consumption ($[\Delta H_2O_2]_A$), as shown in Eq. (1).

$$\eta = \frac{[\Delta H_2O_2]s}{[\Delta H_2O_2]A} \quad (1)$$

The concentration of Fe^{2+} was quantified using UV–vis spectrophotometry at 510 nm with the 1,10-phenanthroline method. The concentration of organic compounds was determined using high performance liquid chromatography (HPLC) with a C18 column. The pseudo-first-order rate constant (k_{obs}) model is introduced to describe the phenols degradation kinetics, as shown in Eq. (2),

$$-\ln\frac{C_t}{C_0} = k_{obs} \times t \quad (2)$$

where C_0 and C_t (mM) are the concentration of phenolic compounds at time 0 and t (min), respectively; k_{obs} is the observed first-order rate constant (min).

3. Results and discussion

3.1. Characterization of the as-prepared CQDs

The preparation process of CQDs is shown in Fig. 1A. When the applied voltage exceeds the electrochemical potential window of water (1.23 V), water decomposes into •OH and •O [42]. Additionally, the addition of HCl significantly enhances the conductivity of the solution, and Cl^- is oxidized to active chlorine ($HClO/ClO^-$) under the influence of the electric field, which gradually damages the graphite structure and leads to the detachment of larger carbon materials [21,33]. These detached carbon materials are attacked by various radicals in the solution, ultimately breaking down into smaller fragments, resulting in the formation of CQDs [34].

As shown in Fig. 1B, the color and yield of the obtained CQDs exhibit

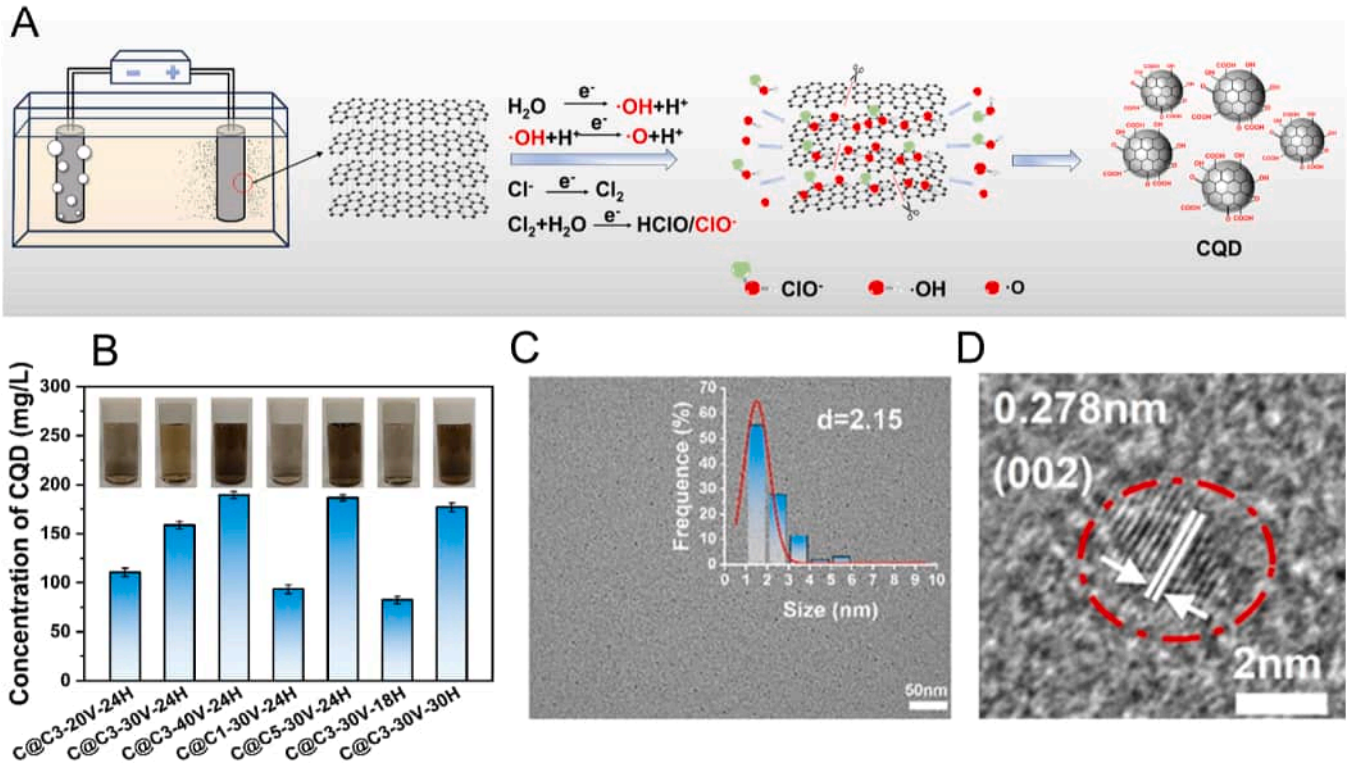

Fig. 1. (A) Schematic illustration of CQDs preparation, (B) concentrations of as-prepared CQDs (inset is the digital photos), (C) TEM and (D) HRTEM image of C@C3–30V-24H (inset in panel C is the particle size distribution).

a "volcanic" variation with increasing voltage, electrolysis time, and electrolyte concentration, peaking at 30 V, 24 hours of electrolysis, and an HCl concentration of 3 mmol/L. When the voltage is too low (less than 30 V), the electrolyte concentration is too low (less than 3 mmol/L), or the electrolysis time is insufficient (less than 24 hours), the number of radicals in the solution is limited, resulting in fewer attacks on larger carbon materials [34]. Consequently, the resulting CQDs tend to be oversized, and these larger CQDs are separated along with the larger carbon materials during purification, leading to reduced yield. On the other hand, when the preparation conditions are excessively harsh, such as when the voltage reaches 40 V, the electrolyte concentration increases to 5 mmol/L, or the electrolysis time extends to 30 hours, the graphite rod undergoes excessive corrosion, leading to the continual detachment of larger carbon materials. Although the number of radicals increases in this case, these free radicals are unable to effectively fragment the larger carbon materials into smaller CQDs, which ultimately are also separated during purification, further decreasing the yield [33].

During the purification process of CQDs, although the purification step effectively separates larger carbon materials, it does not efficiently screen nanoparticle-sized carbon dots by size. Consequently, larger-sized CQDs are retained, which affects their average size and results in relatively larger CQDs when prepared under certain conditions [46]. As shown in Figure S1, when the voltage is set at 30 V, the size of C@C3–30V-24H is smaller than that of C@C3–20V-24H prepared at 20 V, indicating that moderately increasing the voltage can enhance the efficiency of carbon material exfoliation, thereby facilitating the acquisition of smaller CQDs. However, when the voltage is further increased to 40 V, the size of the resulting C@C3–40V-24H increases. Additionally, as the electrolyte concentration and electrolysis duration increase, the size of the CQDs exhibits a similar trend.

Transmission electron microscopy (TEM) images reveal that all CQDs nanoparticles exhibit a quasi-spherical structure and are uniformly dispersed (Fig. 1C, and S1). This observation is in good agreement with earlier reports [44,65]. Statistical analysis of all CQDs revealed that the C@C3–30V-24H shows the smallest average size of 2.15 nm and the narrowest size distribution. Moreover, high-resolution TEM (HRTEM)

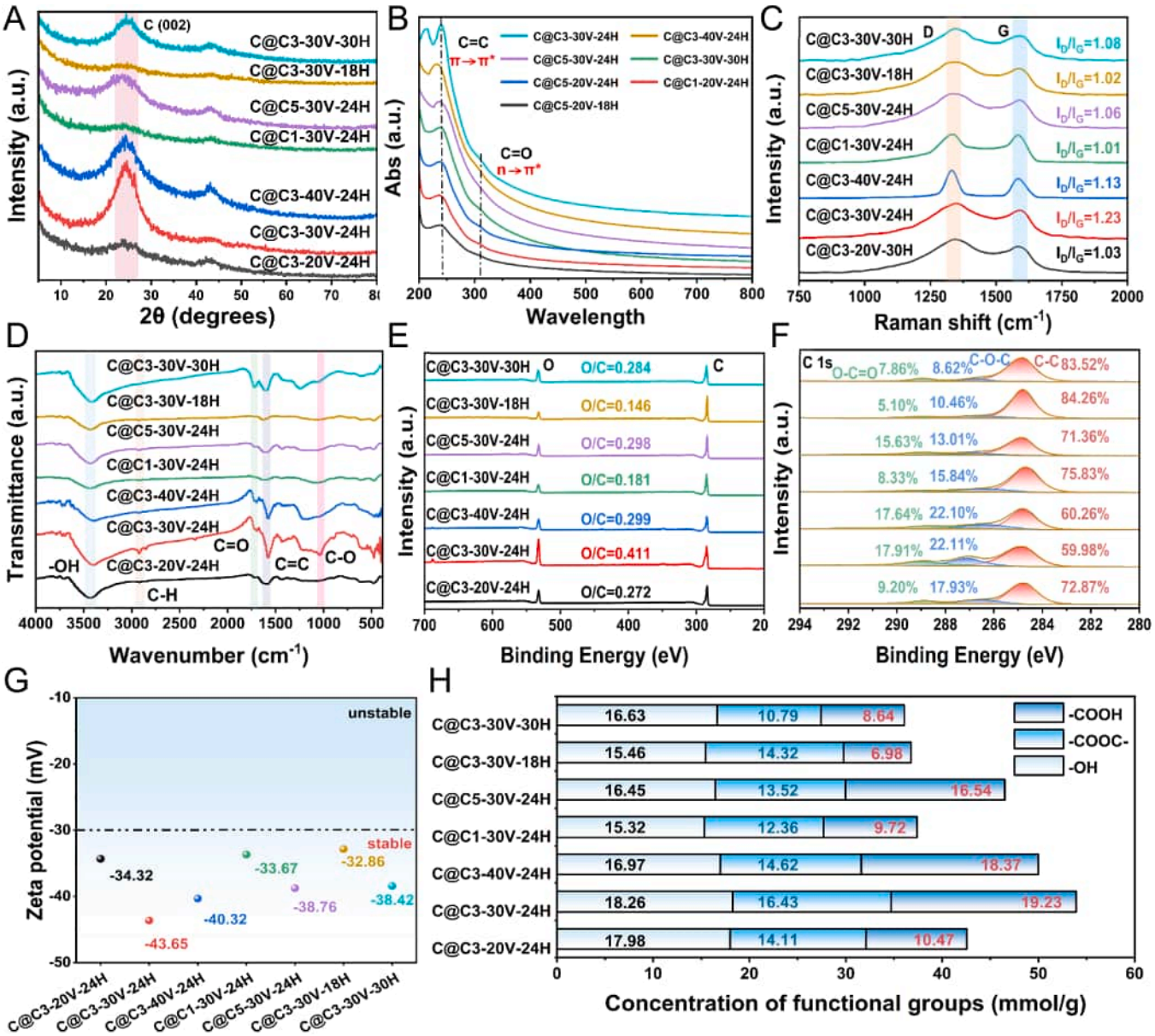

Fig. 2. (A) XRD patterns, (B) UV–vis, (C) Raman, (D) FTIR, (E) XPS, (F) C1s XPS spectra; (G) Zeta potential, and (H) surface functional group compositions of the as-prepared CQDs.

images of all CQDs display distinct lattice fringes (Fig. 1D and S2). The lattice spacings for C@C3–20V-24H, C@C3–30V-24H, C@C3–40V-24H, C@C1–30V-24H, C@C5–30V-24H, C@C3–30V-18H, and C@C3–30V-30H are 0.21, 0.28, 0.25, 0.22, 0.22, 0.20, and 0.22 nm respectively, corresponding to the (100) lattice spacing of graphite [49]. The increase in CQD lattice spacing is believed to be attributed to the insertion of oxygen-containing functional groups into the interlayer of the original CQDs [49]. Note that C@C3–30V-24H demonstrates the largest lattice spacing, implying much more oxygen-containing functional groups inserted.

To further understand the structural evolution of the as-prepared CQDs, we analyzed the X-ray diffraction (XRD) and Raman spectra. As shown in Fig. 2A, all CQDs displayed a broad diffraction peak centered at $2\theta \sim 24.4^{\circ}$, assignable to the (002) lattice plane of carbon-based materials, confirming the nature of graphitic carbon [30]. This observation is also associated with the highly disordered structure of CQDs. The sharpening and narrowing of the diffraction peak may be due to a significant increase in surface functional groups such as C═O, C-O, and -OH under electrochemical conditions. The significant changes in lattice spacing observed in the HRTEM images further support this structural characteristic (Figure S2). Notably, the UV–vis spectra shown in Fig. 2B reveal two fingerprint absorption peaks of CQDs at 242 and 330 nm, respectively, corresponding to the π-π* electronic transition of the conjugated aromatic sp^2 hybridized C═C bonds within the graphite core, and the n-π* transition of the C═O bonds in COOH groups [36].

The Raman spectra (Fig. 2C) feature two prominent peaks at 1350 and 1620 cm^{-1}, respectively, which belong to the D-band and G-band characteristic peaks of carbon materials, respectively. The G-band is closely related to the in-plane vibrations of sp^2 hybridized carbon atoms, while the D-band primarily reflects the presence of topological defects or sp^3 hybridized carbon atoms [49]. Therefore, by evaluating the intensity ratio of the D-band to the G-band (I_D/I_G), we can effectively infer the defect levels of carbon materials [35]. During the experiment, where the electrolyte concentration and electrolysis time were constant and the voltage was gradually increased from 20 to 40 V, the I_D/I_G ratio initially experienced a significant increase from 1.03 to 1.23, followed by a slight decrease to 1.06. Similarly, when the electrolyte concentration was increased from 1 to 5 mmol/L, or the electrolysis time was extended from 18 hours to 30 hours, the I_D/I_G ratio also exhibited a trend of first increasing and then decreasing, with values of 1.06 and 1.08, respectively. These observations collectively indicate that the formation of structural defects accompanies the electrochemical exfoliation of graphite to prepare CQDs, with the sp^2 domains in the C@C3–30V-24H sample exhibiting the most significant defect characteristics. The Fourier-transform infrared (FT-IR) spectra (Fig. 2D) further refine the information on functional groups, with a typical peak around 3450 cm^{-1} corresponding to the stretching vibration of -OH, and a peak at 2920 cm^{-1} attributed to the stretching vibration of C-H in $-CH_3$ or $-CH_2$ groups. The peak at 1686 cm^{-1} indicates the presence of carbonyl (C═O), and the peak at 1580 cm^{-1} reflects the stretching vibration of sp^2 hybridized C═C groups, while the peak at 1050 cm^{-1} is associated with C-O bonds [49]. The presence of these oxygen-containing groups is direct evidence of successful graphite oxidation and imparts hydrophilicity to CQDs. X-ray photoelectron spectroscopy (XPS) measurements further revealed the oxygen-containing functional groups in CQDs, as shown in Fig. 2E. The C 1 s (284.8 eV) and O 1 s (532.4 eV) peaks in the XPS spectra indicate that all CQDs consist of carbon and oxygen elements. The increase in the O/C atomic ratio directly reflects the enhancement of the oxidation degree of CQDs. Among the seven samples, C@C3–30V-24H had the highest O/C ratio of 0.411, indicating increased oxygen content. Deconvolution of the C 1 s spectrum revealed three peaks at 284.8 eV, 286.6 eV, and 288.9 eV, corresponding to C-sp^2, C-O, and C═O, respectively (Fig. 2F) [35]. The results indicate that C═O and C-O are the primary oxygen-containing groups in CQDs, with C-O bonds dominating the oxygen element composition, although the content of C═O bonds is also substantial. Among the seven tested CQDs, C@C3–30V-24H had the lowest C-sp^2 content, indicating the highest degree of oxidation and the highest C═O content. This high C═O content may be key to improving Fenton-like catalytic activity.

The zeta potential was measured to study the surface charge properties of these CQDs. All CQDs exhibited negative potentials, ranging from −32.86 to −43.65 mV (Fig. 2G), confirming the stability of the CQDs colloids, as colloids are generally stable with zeta potentials above 30 mV (positive or negative). The zeta potential of CQDs colloids is mainly attributed to the extensive distribution of carboxyl functional groups on their surfaces, which impart negative charge characteristics to CQDs. The higher the carboxyl content, the higher the hydrophilicity and stability of CQDs colloids [65]. Additionally, the concentrations of oxygen-containing functional groups, particularly carboxyl groups, in each CQDs sample were accurately quantified using Boehm titration, as illustrated in Fig. 2H. The C@C3–30V-24H sample exhibited the highest carboxyl content, a finding that is highly consistent with the Zeta potential analysis results, further confirming the close relationship between its surface chemical properties and stability. Notably, these results demonstrate that the chemical compositions and oxygen-containing functional groups of all CQDs are similar and that the carboxyl content of CQDs is proportional to their $\boldsymbol{k}_{obs}$ (R^2=0.948) while showing poor linear correlations with -COO- (R^2=0.420) and -OH (R^2=0.440) (Figure S3). This indicates that carboxyl groups are the primary factor influencing the efficiency of Fenton-like reactions, which is consistent with reports elsewhere [35,65]. The -COOH groups form complexes with Fe^{3+}, facilitating electron transfer and accelerating the Fe^{2+}/ Fe^{3+} cycle, which is essential for enhancing the Fenton-like catalytic effect.

3.2. CQDs-assisted Fenton-like catalysis

To evaluate the performance of various CQDs-Fe^{3+} complexes, their efficacy was assessed in the CQDs-Fe^{3+}/H_2O_2 system for phenol degradation. As depicted in Fig. 3A, the C@C3–30V-24H complex demonstrated the most effective co-catalytic performance, achieving a phenol degradation efficiency of 97.75 % within 15 minutes. Furthermore, it exhibited the highest observed rate constant $\boldsymbol{k}_{obs}$ of 0.2597 min^{-1} (Fig. 3B). Due to the strong correlation between the chemical cycling behavior of Fe^{2+}/Fe^{3+} and the pH of the reaction system [12], we measured the pH changes in various CQDs-Fe^{3+}/H_2O_2 systems throughout the experiment, as illustrated in Figure S4. It was observed that the pH values in each reaction system exhibited a slight decrease during the reaction period, with a change of less than 0.04. This variation is considered negligible in terms of its impact on the conversion of Fe^{2+}/Fe^{3+} [19]. We systematically explored the phenol degradation performance in various systems, as presented in Fig. 3C. The degradation efficiency of phenol was relatively low in systems containing only Fe^{3+}, only H_2O_2, only C@C3–30V-24H, Fe^{3+}/H_2O_2, and C@C3–30V-24H/H_2O_2. In contrast, the C@C3–30V-24H-Fe^{3+}/H_2O_2 system demonstrated significantly higher phenol degradation efficiency. The low efficiency in the Fe^{3+}/H_2O_2 system was attributed to iron ion hydrolysis, which severely hindered the Fe^{3+}/Fe^{2+} redox cycle, resulting in a sluggish degradation reaction. However, in the C@C3–30V-24H-Fe^{3+}/H_2O_2 system, CQDs effectively suppressed iron ion hydrolysis and significantly accelerated the Fe^{3+}/Fe^{2+} cycle through enhanced electron transfer, thereby achieving efficient phenol degradation [65].

It is well known that the core difference between the Fe^{3+}/H_2O_2 and Fe^{2+}/H_2O_2 systems lies in the initial step of Fe^{3+} to Fe^{2+} conversion. Subsequently, these two systems exhibit similar reaction progressions, making the Fe^{3+} to Fe^{2+} conversion rate a key factor influencing the reaction process [26]. Given that phenol is a recognized Fe^{3+} complexing agent and reducing agent [66], we measured the generation of Fe^{2+} and the consumption of H_2O_2 in both the presence and absence of phenol to elucidate its role in iron cycling, as illustrated in Figure S5. The results demonstrated that the presence of phenol in the Fe^{3+}/H_2O_2

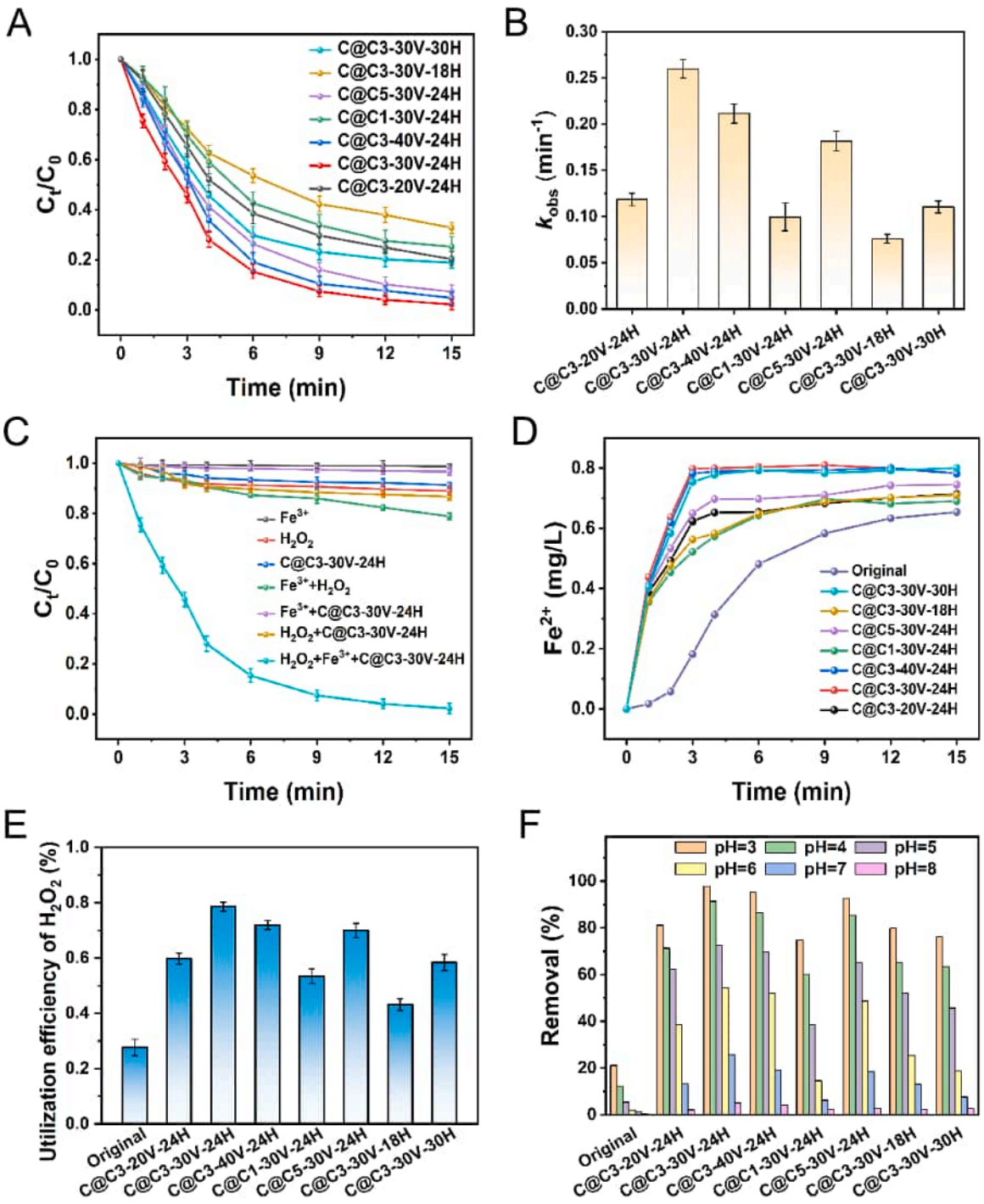

Fig. 3. (A) Phenol degradation kinetics in different CQDs-Fe^{3+}/H_2O_2 systems, (B) comparison of the corresponding apparent rate constant k_{obs}, (C) comparison of phenol degradation kinetics in different systems, (D) changes in Fe^{2+} concentration over time, (E) comparison of H_2O_2 utilization efficiency, (F) comparison of phenol removal% in different CQD-Fe^{3+}/H_2O_2 systems at pH 3 −8 (CQDs = 2 mg/L, Fe^{3+} = 2 mg/L, H_2O_2 = 5 mmol/L, phenol = 10 mg/L).

system accelerates the conversion of Fe^{3+} to Fe^{2+}, while the consumption of H_2O_2 also increased, which is consistent with previous studies [1, 11]. Furthermore, the addition of C@C3–30V-24H further enhanced the transformation of Fe^{3+} to Fe^{2+} and resulted in a higher consumption of hydrogen peroxide due to the rapid degradation of pollutants compared to the previous conditions. The temporal variation of Fe^{2+} concentrations in different CQDs-Fe^{3+}/H_2O_2 systems is shown in Fig. 3D. The Fe^{2+} concentration in the CQDs-Fe^{3+}/H_2O_2 system rapidly increased within the first 3 minutes and then remained stable with a slight increase from 3 to 15 minutes. Conversely, in the Fe^{3+}/H_2O_2 system, the Fe^{2+} concentration slowly increased over 15 minutes, indicating that CQDs facilitated the Fe^{2+} generation kinetics. The C@C3–30V-24H sample possesses the highest carboxyl content, leading to the most extensive complexation with Fe^{3+}. It's believed that enhancing the Fe^{2+}/Fe^{3+} conversion rate can significantly improve H_2O_2 utilization efficiency [45]. Therefore, we quantitatively analyzed the H_2O_2 utilization efficiency in different CQDs-Fe^{3+}/H_2O_2 systems. As illustrated in Fig. 3E, the H_2O_2 utilization efficiency in the Fe^{3+}/H_2O_2 system was only 27.64 % after 15 minutes of reaction. In contrast, the CQDs-Fe^{3+}/H_2O_2 systems significantly improved H_2O_2 utilization efficiency, with the

C@C3–30V-24H-Fe^{3+}/H_2O_2 system achieving 78.54 %, which is 2.84 times higher than the Fe^{3+}/H_2O_2 system, and 1.8 and 1.47 times higher than the C@C3–24V-30H and C@C1–24V-30H systems, respectively.

Conventional Fenton-like reactions are typically limited to acidic conditions. However, most real-world wastewater is neutral or alkaline [15]. Therefore, pH is a critical factor for the practical application of Fenton-like reactions. Simultaneously, we investigated the changes in pH within each reaction system and observed that as the reaction progressed, the pH values decreased compared to the initial pH; however, the magnitude of this change was not significant (Figure S6). This finding suggests that the initial pH plays a critical role in Fenton-like reactions. Notably, the C@C3–30V-24H, C@C3–40V-24H, and C@C5–30V-24H systems maintained approximately 50 % degradation efficiency at pH 6. This is due to the increase in pH which facilitates the decomposition of H_2O_2 into HOO^- and O_2, making the generation of •OH more challenging. Nonetheless, the carboxyl groups that are extensively present on the surface of CQDs assume a critical role. These carboxyl groups impart an exceptional buffering capacity, thereby effectively suppressing the hydrolysis of iron ions in an alkaline environment. Consequently, this suppression facilitates the progression of the Fe^{3+}/Fe^{2+} redox cycle, thereby expanding the pH operational range of the CQDs-Fe^{3+}/H_2O_2 system [35,65]. However, when the pH exceeds 7, the phenol removal efficiency drops sharply due to excessive hydrolysis of Fe^{3+}, which exceeds the buffering capacity of CQDs. In summary, under pH conditions ≥ 4, the CQDs-Fe^{3+}/H_2O_2 systems demonstrate significantly better phenol degradation performance compared to traditional Fe^{3+}/H_2O_2 systems.

3.3. The effects of the reaction parameter

As shown in Fig. 4A, increasing the H_2O_2 concentration from 1 mmol/L to 5 mmol/L led to the effective decomposition of H_2O_2 into •OH and •O_2H, thereby increasing the phenol removal efficiency from 36.94 % to 97.75 % and the reaction kinetic constant from 0.0304 min^{-1} to 0.2597 min^{-1} (Figure S7). However, further increases in H_2O_2 concentration to 10 mmol/L and 20 mmol/L resulted in inhibitory reactions, reducing the phenol degradation efficiency to 95.31 % and 78.83 %, respectively. Hence, the optimal H_2O_2 concentration was determined to be 5 mmol/L. This phenomenon can be attributed to the fact that a moderate increase in H_2O_2 promotes the generation of •OH, whereas an excess of H_2O_2 reacts with •OH to form •O_2H, as illustrated by the reaction equation $H_2O_2 + •OH \rightarrow H_2O + •O_2H$ [63]. The redox potential of •O_2H (1.44 V) is significantly lower than that of •OH (2.8 V), thereby inhibiting phenol decomposition when H_2O_2 is in excess [3,38]. Fig. 4B illustrates the effect of C@C3–30V-24H concentration on phenol degradation. As the C@C3–30V-24H concentration increased from 0.1 to 2 mg/L, the number of carboxyl groups participating in complexation with Fe^{3+} also increased, enhancing the solution's buffering capacity and accelerating the Fe^{3+}/Fe^{2+} cycle. Consequently, the phenol removal efficiency increased from 71.85 % to 97.75 %, and the k_{obs} increased from 0.0871 min^{-1} to 0.2597 min^{-1}. When the concentration reached 4 mg/L, the electron-rich C@C3–30V-24H quenched the •OH produced in the reaction, reducing the phenol degradation efficiency to 92.91 %. Therefore, the optimal concentration of C@C3–30V-24H was determined to be 2 mg/L.

Fig. 4 C examines the impact of Fe^{3+} concentration. When the Fe^{3+} concentration reached 2 mg/L, the phenol degradation performance was optimal, with a removal efficiency of 97.75 %. At lower Fe^{3+} concentrations, hydrolysis reactions led to poor catalytic performance of H_2O_2. Conversely, at higher Fe^{3+} concentrations, clustering occurred between C@C3–30V-24H and Fe^{3+}, inhibiting its catalytic activity and reducing the phenol degradation efficiency [35]. Thus, the optimal Fe^{3+} concentration was determined to be 2 mg/L.

In real wastewater, various inorganic anions typically coexist with

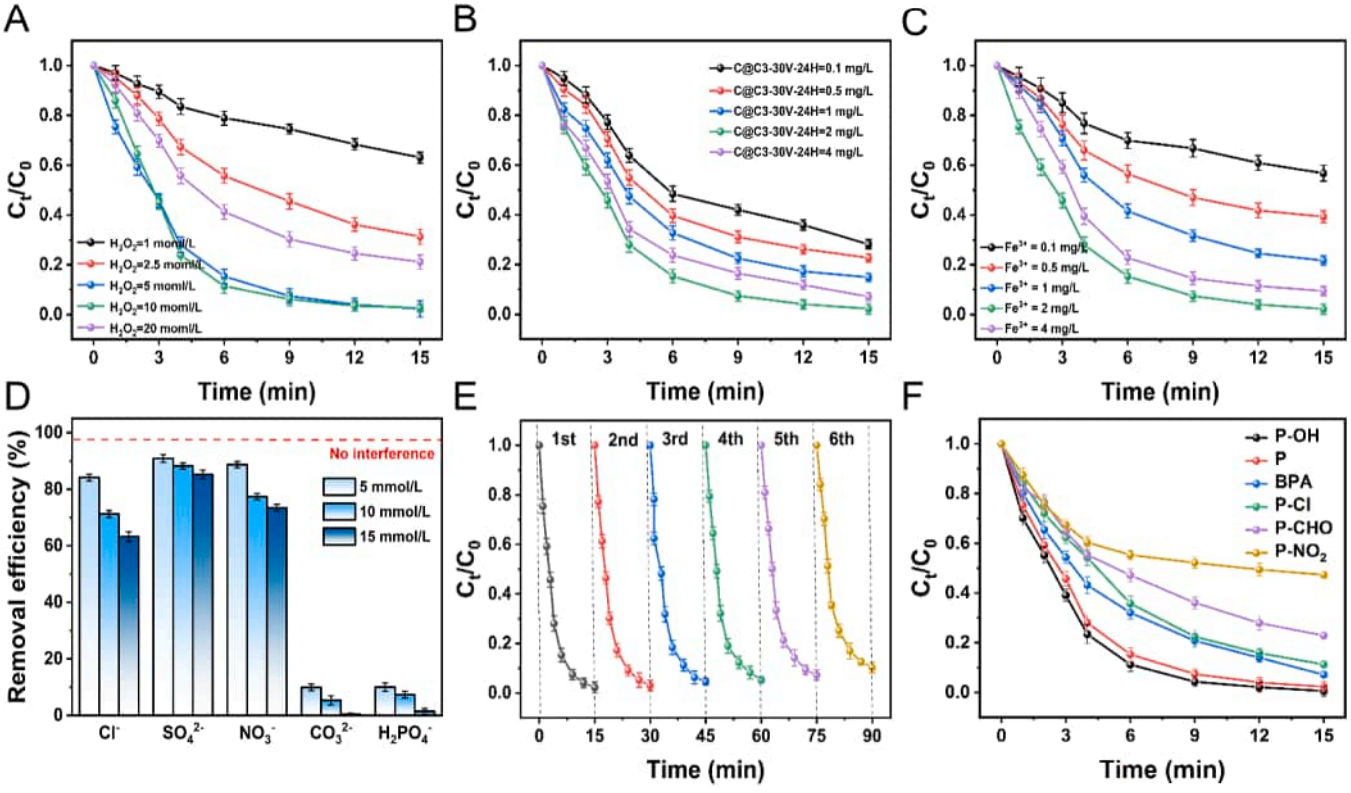

Fig. 4. The effects of (A) H_2O_2, (B) C@C3–30V-24H dosage, and (C) Fe^{3+}, on the phenol degradation kinetics in C@C3–30V-24H-Fe^{3+}/H_2O_2 system; (D) the impacts of different anions on phenol degradation, (E) the cycling performance of C@C3–30V-24H, (F) degradation kinetics of six phenolic compounds over the C@C3–30V-24H-Fe^{3+}/H_2O_2 system (hydroquinone (P-OH), phenol (P), bisphenol A (BPA), para-chlorophenol (P-Cl), para-hydroxybenzaldehyde (P-CHO), and para-nitrophenol (P-NO_2) = 10 mg/L, CQDs = 2 mg/L, Fe^{3+} = 2 mg/L, H_2O_2 = 5 mmol/L, phenol = 10 mg/L, pH = 3).

the target pollutants. The performance of the oxidation process may be affected by these coexisting components. Therefore, to evaluate their effects, we investigated the influence of coexisting anions such as Cl^-, SO_4^{2-}, NO_3^-, CO_3^{2-}, and $H_2PO_4^-$ on phenol removal efficiency in the C@C3–30V-24H-Fe^{3+}/H_2O_2 system under optimal conditions. Fig. 4D depicts the phenol removal efficiency in the presence of 5–15 mmol/L of these anions and cations. Among the coexisting anions, CO_3^{2-} and $H_2PO_4^-$ exhibited higher inhibitory effects compared to Cl^-, SO_4^{2-}, and NO_3^-. At a concentration of 5 mmol/L, the phenol removal efficiency decreased from 97.75 % to 9.91 % and 10.02 % for CO_3^{2-} and $H_2PO_4^-$, respectively, after 15 minutes of reaction. In contrast, at a concentration of 15 mmol/L, Cl^-, SO_4^{2-}, and NO_3^- only slightly inhibited phenol degradation, maintaining over 60 % degradation efficiency. Generally, the inhibitory effects of anions arise from two main sources. First, they act as •OH radical scavengers, appearing in the form of weaker radicals with lower redox potentials ($ClOH^-$•, Cl•, NO_3•, CO_3^-•, H_2PO_4•) [3], as shown in Eq. (3)–(7):

$$Cl^- + \bullet OH \rightarrow ClOH\bullet^-/Cl\bullet \quad (3)$$

$$SO_4^{2-} + \bullet OH \rightarrow SO_4^-\bullet + OH^- \quad (4)$$

$$NO_3^- + \bullet OH \rightarrow NO_3\bullet + OH^- \quad (5)$$

$$HCO_3^- + \bullet OH \rightarrow H_2O + CO_3^-\bullet \quad (6)$$

$$H_2PO_4^- + \bullet OH \rightarrow H_2PO_4\bullet + OH^- \quad (7)$$

Second, they cause changes in the solution's pH, thereby affecting the stability of H_2O_2 and •OH. High concentrations of HCO_3^-/$H_2PO_4^-$ can act as buffering agents, promoting hydrolysis reactions and shifting the equilibrium to the right, as shown in the reaction equations below. Additionally, $H_2PO_4^-$ can bind with Fe^{2+}/Fe^{3+}, rendering the catalyst inactive, as shown in the Eqs. (8)-(11). This prevents CQD from adsorbing and cycling Fe^{2+}/Fe^{3+}, and from activating H_2O_2, thereby significantly inhibiting phenol degradation [6].

$$HCO_3^- + H_2O \Leftrightarrow H_2CO^{3+}OH^- \quad (8)$$

$$H_2PO_4^- + H_2O \Leftrightarrow H_3PO_4 + OH^- \quad (9)$$

$$Fe^{2+} + H_2PO_4^- \rightarrow FeH_2PO_4^+ \quad (10)$$

$$Fe^{3+} + H_2PO_4^- \rightarrow FeH_2PO_4^{2+} \quad (11)$$

The reproducibility and versatility of C@C3–30V-24H are important indicators for treating actual wastewater. To determine its reproducibility, we allowed the completed experiment to stand for 10 days to ensure complete degradation of phenol and intermediate products [65]. For each new cycle experiment, new phenol (10 mg/L) and additional H_2O_2 and Fe^{3+} were added to match the initial experimental conditions. As shown in Fig. 4E, six cycles were performed. Although the phenol removal efficiency decreased with each cycle, it remained around 90 %, indicating good cyclic stability of C@C3–30V-24H. Additionally, we investigated the degradation performance of the C@3–30V-24H-Fe^{3+}/H_2O_2 system for various phenolic pollutants. As illustrated in Fig. 4F, within 15 minutes, the removal efficiencies of hydroquinone (P-OH), phenol (P), bisphenol A (BPA), p-chlorophenol (P-Cl), p-hydroxybenzaldehyde (P-CHO), and p-nitrophenol (P-NO_2) were 99.41 %, 97.57 %, 92.84 %, 88.73 %, 77.19 %, and 52.68 %, respectively, indicating superior degradation performance. These results indicate that the C@3–30V-24H-Fe^{3+}/H_2O_2 system exhibits significant potential for the treatment of complex organic wastewater.

3.4. Active species

To elucidate the reactive species generated within the C@3–30V-24H-Fe^{3+}/H_2O_2 system, we conducted quenching experiments and electron paramagnetic resonance (EPR) analysis. Fig. 5 A,B illustrate that tert-butanol (TBA) serves as a typical scavenger for •OH [37], while 2,2,6,6-tetramethyl-4-piperidinyloxy (TEMPOL) and furfuryl alcohol (FFA) demonstrate effective scavenging capabilities for HO_2•/•O_2^- and $^1O_2$, respectively [18,22]. As shown in Figure S8A, a TBA concentration of 10 mM significantly inhibited phenol degradation, indicating that •OH plays a decisive role in this process. EPR spectral analysis revealed that the DMPO−•OH signal (1:2:2:1) intensity in the C@3–30V-24H-Fe^{3+}/H_2O_2 system was notably higher than in the Fe^{3+}/H_2O_2 system, suggesting that the former generates more •OH. This evidence supports the critical role of •OH in phenol degradation within this system.

At a TEMPOL concentration of 5 mM, its inhibitory effect on phenol removal efficiency was negligible (Figure S8B), and likewise, the addition of FFA did not result in significant inhibition (Figure S8C). Notably, increasing the TEMPOL concentration to 20 mM somewhat inhibited phenol removal (Figure S8B). This could be attributed to the partial quenching of •OH, since quenching agents may react with multiple oxidants, and no truly selective quenching agents exist [62]. These results suggest that HO_2•/•O_2^- and $^1O_2$ play a minor role in this system. To evaluate the potential impact of high-valent iron species (Fe(IV)) in the C@3–30V-24H-Fe^{3+}/H_2O_2 system [54], dimethyl sulfoxide (DMSO) was introduced since it is a sensitive compound that can be selectively oxidized by high-valent metals through oxygen atom transfer reactions

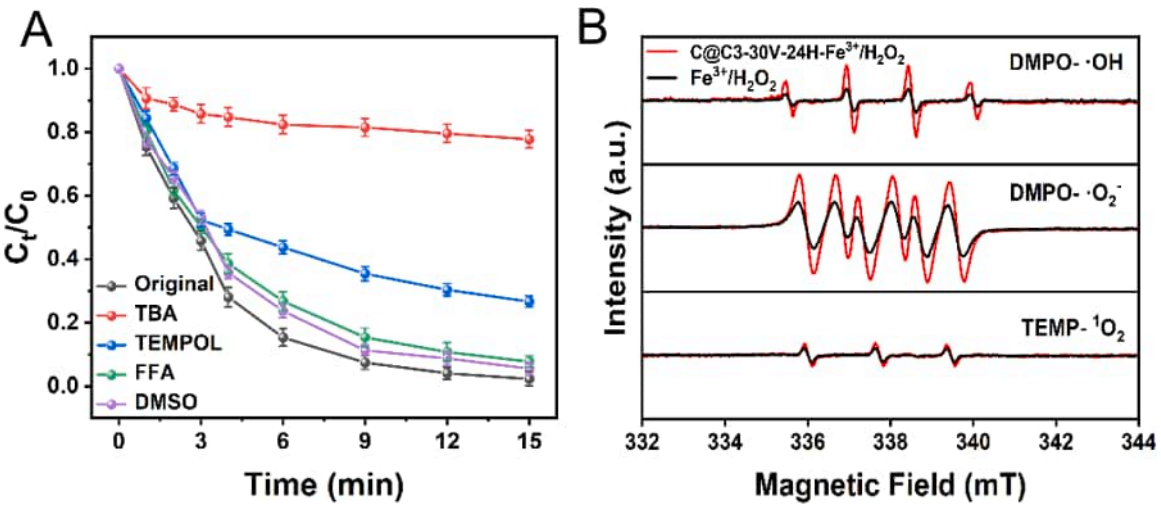

Fig. 5. (A) The effects of varying scavengers on phenol degradation in the C@C3–30V-24H-Fe^{3+}/H_2O_2 system, (B) spin trapping EPR spectra of DMPO−·OH, DMPO−·O_2^-, and TEMP−$^1O_2$ in both the C@C3–30V-24H-Fe^{3+}/H_2O_2 and the Fe^{3+}/H_2O_2 systems.

and is commonly used as a quencher for Fe(IV) [22]. Increasing the DMSO concentration from 5 mM to 20 mM (Figure S8D) resulted in no significant inhibition of phenol removal, suggesting that high-valent iron species are not the primary active species in this system.

3.5. Relationship between degradation performances and properties of pollutants

Fig. 6A illustrates the structural diagrams of six contaminants along with their k_{obs} in the C@3–30V-24H-Fe^{3+}/H_2O_2 system. The data reveal that pollutants containing electron-donating groups such as hydroxyl (OH) for instance, P-OH, P, and BPA are more readily oxidized in this system, exhibiting k_{obs} values exceeding 0.16 min^{-1}. In contrast, pollutants possessing electron-withdrawing groups, such as P-Cl, P-CHO, and P-NO_2, demonstrate lower oxidation efficiency, with k_{obs} values under 0.16 min^{-1}. In the Fenton-like system involving six pollutants, the variation in Fe^{2+} concentration is illustrated in Figure S9. The results indicate that the addition of C@C3–30V-24H results in a general increase in Fe^{2+} concentrations. Notably, the concentration of Fe^{2+} in systems containing electron-donating groups is consistently higher than that in systems with electron-withdrawing groups (Figure S10A). Furthermore, we observed a significant correlation between Fe^{2+} concentrations and the k_{obs} values. Specifically, as the concentration of Fe^{2+} in the reaction system increases, the k_{obs} values for pollutant degradation also increase (Figure S10A,B). This indicates that the type of electronic groups in pollutants significantly influences

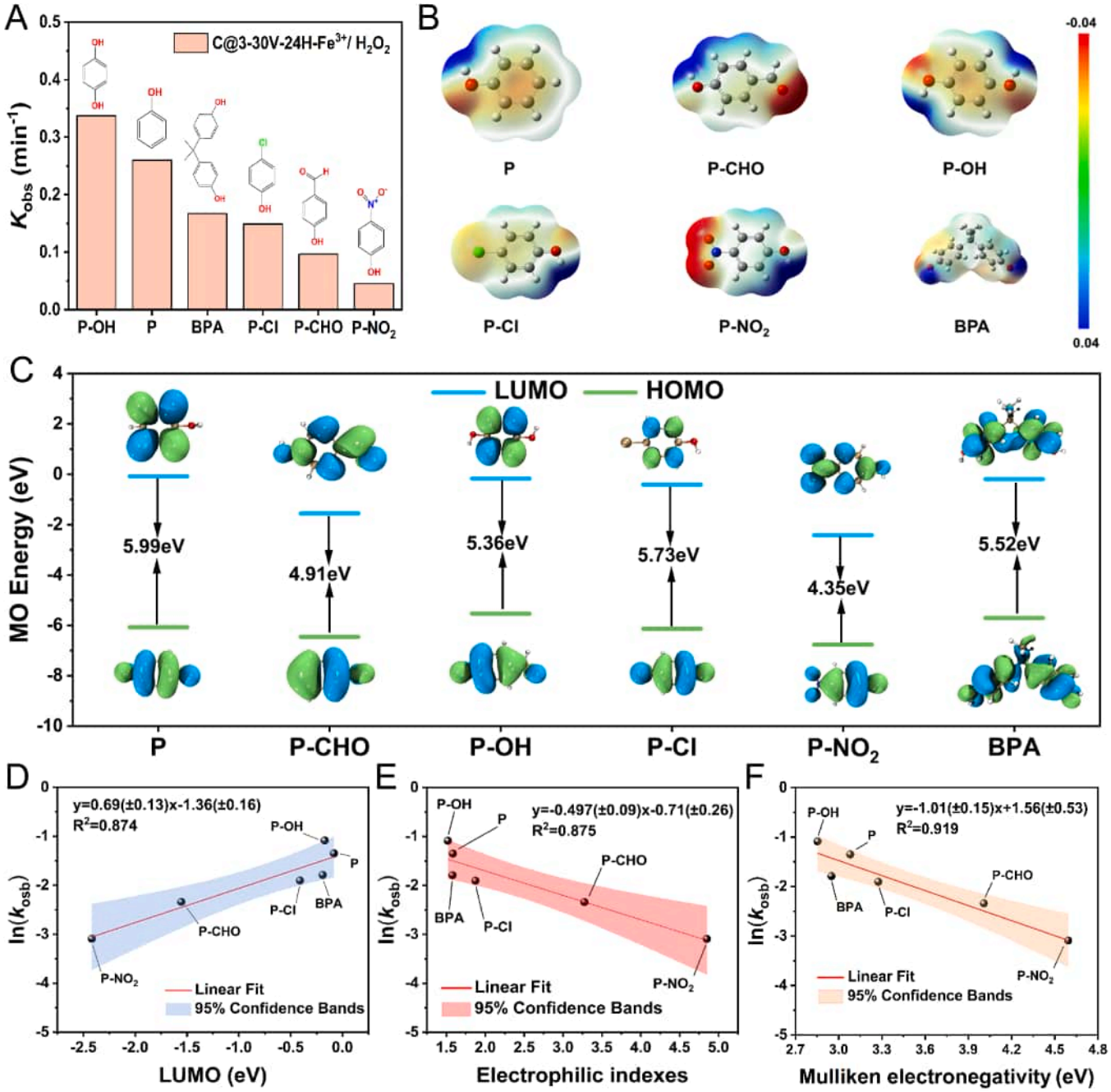

Fig. 6. (A) Comparison of k_{obs} obtained from phenolic pollutant degradation in the C@C3–30V-24H-Fe^{3+}/H_2O_2 system, (B) electrostatic potential distribution of the phenolic compounds, (C) LUMO and HOMO energy levels of the pollutants; the linear correlations between (D) the LUMO, (E) the electrophilicity index, and (F) the Mulliken electronegativity and the corresponding ln(k_{obs}) in the C@C3–30V-24H-Fe^{3+}/H_2O_2 system.

the reduction efficiency of Fe^{3+}, subsequently affecting the degradation efficacy of the pollutants [66]. Fig. 6B depicts the electrostatic potential distribution for six phenolic pollutants, generated using GaussView 6.0 software [10]. The red regions indicate the areas with the highest negative potential, whereas the blue regions denote the areas with positive potential. The results indicate that substituents exert different influences on the electrostatic potential distribution surrounding the benzene ring and hydroxyl group. Generally, the most electronegative regions are localized around the oxygen atoms, including the −OH groups and their attached substituents, whereas the most electropositive regions are concentrated on the hydrogen atoms of the —OH groups [27].

To further elucidate the relationship between contaminant properties and degradation performance, this study employed the Gaussian 16 software package and density functional theory (DFT) calculations to analyze additional parameters of various contaminants [14]. These parameters encompass the electrophilicity index, highest occupied molecular orbital (HOMO), lowest unoccupied molecular orbital (LUMO), and Mulliken electronegativity. Further analyses of HOMO and LUMO were conducted using the Multiwfn wavefunction analysis program [40, 41]. Fig. 6C showcases the LUMO and HOMO energy levels of the six contaminants, and the LUMO-HOMO energy gap (E_{LUMO}-E_{HOMO}) was calculated and presented in Figure S11. This gap represents the energy required to transfer electrons from the HOMO to the LUMO. Although E_{LUMO}-E_{HOMO} provides initial insights into the electronic structure of the molecules, it exhibits a poor linear correlation with ln($\boldsymbol{k}_{obs}$) in the C@3–30V-24H-Fe^{3+}/H_2O_2 system (R^2=0.677), rendering it ineffective for correlating with the degradation performance of the pollutants.

The LUMO energy level reflects a molecule's electron-accepting capability. A higher LUMO energy level implies that the pollutant requires more energy to accept electrons [17]. The data in Fig. 6D demonstrate that pollutants with lower LUMO energy levels exhibit a strong linear correlation with ln($\boldsymbol{k}_{obs}$) (R^2=0.889). The electrophilicity index measures the tendency of a pollutant to accept electrons. Pollutants with a lower electrophilicity index display reduced electron-accepting ability and increased electron-donating capacity. Fig. 6E indicates that the electrophilicity index correlates well with ln ($\boldsymbol{k}_{obs}$) (R^2=0.891). Specifically, pollutants with lower electrophilicity indices, such as P-OH, P, and BPA, show higher ln($\boldsymbol{k}_{obs}$) values in the C@3–30V-24H-Fe^{3+}/H_2O_2 system. Mulliken electronegativity indicates a pollutant's ability to attract electrons. Fig. 6F reveals an excellent linear correlation between Mulliken electronegativity and ln($\boldsymbol{k}_{obs}$) (R^2=0.919), suggesting that higher Mulliken electronegativity signifies a greater propensity for the pollutant to attract and retain electrons. This, in turn, inhibits the transfer of electrons to active species (such as •OH) during the degradation process, resulting in a slower reaction efficiency [2].

4. Conclusions

In summary, this study utilized electrochemical exfoliation to precisely control the surface functional group concentration of CQDs and systematically examined their co-catalytic performance in Fenton-like reactions. The system C@3–30V-24H-Fe^{3+}/H_2O_2 exhibited superior catalytic activity, a broadly applicable pH range, and a high Fe^{3+}/Fe^{2+} conversion rate. Furthermore, C@3–30V-24H- Fe^{3+}/H_2O_2 demonstrated significant reusability and versatility, indicating substantial application potential. DFT calculations revealed that pollutants with low LUMO energy levels and low electrophilicity indices are more readily oxidized, whereas high Mulliken electronegativity inhibits electron transfer to active species. These findings provide theoretical support for predicting the degradation performance of various pollutants in the C@3–30V-24H-Fe^{3+}/H_2O_2 system. In conclusion, by controlling the preparation parameters, this study precisely regulated the yield and carboxyl content of CQDs, predicted the degradation performance of different pollutants in the C@3–30V-24H-Fe^{3+}/H_2O_2 system, and offered unique insights into the CQDs-Fe^{3+}/H_2O_2 system

Environmental implication

As industrialization intensifies, the excessive discharge of refractory phenolic pollutants from wastewater in industries such as petrochemical and pharmaceutical sectors have led to increased water pollution, which has adversely affected human and environmental health. This work offers insights into how the preparation conditions affect the cocatalytic performance of CQDs for phenol decomposition, underscoring their role as cocatalysts in Fenton-like processes, improving the efficiency of phenolic pollutant removal, and promoting environmental sustainability.

CRediT authorship contribution statement

Xia Yangfan: Writing – original draft, Visualization, Validation, Methodology, Investigation, Formal analysis, Data curation. **Huang Xu:** Resources, Data curation. **Wu Kaiqiang:** Methodology, Investigation. **Tian Yechao:** Methodology, Data curation. **Shen Yifan:** Software, Resources. **Zhang Jifa:** Investigation. **Chen Yongjie:** Data curation. **Li Dawei:** Writing – review & editing, Supervision, Funding acquisition, Conceptualization. **Li Feihu:** Writing – review & editing, Visualization.

Declaration of Competing Interest

The authors declare that they have no known competing financial interests or personal relationships that could have appeared to influence the work reported in this paper.

Acknowledgments

The work was financially supported by the National Natural Science Foundation of China (NSFC, 52000101).

Appendix A. Supporting information

Supplementary data associated with this article can be found in the online version at doi:10.1016/j.jhazmat.2025.137607.

Data availability

Data will be made available on request.

References

[1] Ahmad, M., Teel, A.L., Watts, R.J., 2013. Mechanism of persulfate activation by phenols. Environ Sci Technol 47 (11), 5864–5871. https://doi.org/10.1021/es400728c.
[2] Al-Sehemi, A.G., Irfan, A., 2017. Effect of donor and acceptor groups on radical scavenging activity of phenol by density functional theory. Arab J Chem 10, S1703–S1710. https://doi.org/10.1016/j.arabjc.2013.06.019.
[3] Armstrong, D.A., Huie, R.E., Koppenol, W.H., Lymar, S.V., Merényi, G., Neta, P., Ruscic, B., Stanbury, D.M., Steenken, S., Wardman, P., 2015. Standard electrode potentials involving radicals in aqueous solution: inorganic radicals (IUPAC Technical Report). Pure Appl Chem 87 (11-12), 1139–1150. https://doi.org/10.1515/pac-2014-0502.
[4] Babuponnusami, A., Muthukumar, K., 2014. A review on Fenton and improvements to the Fenton process for wastewater treatment. J Environ Chem Eng 2 (1), 557–572. https://doi.org/10.1016/j.jece.2013.10.011.
[5] Chen, X., Fu, W., Yang, Z., Yang, Y., Li, Y., Huang, H., Zhang, X., Pan, B., 2023. Enhanced H_2O_2 utilization efficiency in Fenton-like system for degradation of emerging contaminants: oxygen vacancy-mediated activation of O_2. Water Res 230, 119562. https://doi.org/10.1016/j.watres.2022.119562.
[6] Cheng, X., Liang, L., Ye, J., Li, N., Yan, B., Chen, G., 2023. Influence and mechanism of water matrices on H_2O_2-based Fenton-like oxidation processes: a review. Sci Total Environ 888, 164086. https://doi.org/10.1016/j.scitotenv.2023.164086.
[7] Choi, J., Choi, M.J., Kim, J., Dinic, F., Todorovic, P., Sun, B., Wei, M., Baek, S.W., Hoogland, S., Garcia de Arquer, F.P., Voznyy, O., Sargent, E.H., 2020. Stabilizing surface passivation enables stable operation of colloidal quantum dot photovoltaic

devices at maximum power point in an air ambient. Adv Mater 32 (7), e1906497. https://doi.org/10.1002/adma.201906497.
[8] Deng, F., Olvera-Vargas, H., Zhou, M., Qiu, S., Sires, I., Brillas, E., 2023. Critical review on the mechanisms of Fe^{2+} regeneration in the electro-fenton process: fundamentals and boosting strategies. Chem Rev 123 (8), 4635–4662. https://doi.org/10.1021/acs.chemrev.2c00684.
[9] Deng, G., Wang, Z., Ma, J., Jiang, J., He, D., Li, X., Szczuka, A., Zhang, Z., 2023. Ferryl ion in the photo-fenton process at acidic pH: occurrence, fate, and implications. Environ Sci Technol 57 (47), 18586–18596. https://doi.org/10.1021/acs.est.2c06373.
[10] Dennington R., Keith T.A., Millam J.M., GaussView, version 6.0. 16. Semichem Inc Shawnee Mission KS; 2016.
[11] Du, Y., Zhou, M., Lei, L., 2006. Role of the intermediates in the degradation of phenolic compounds by Fenton-like process. J Hazard Mater 136 (3), 859–865. https://doi.org/10.1016/j.jhazmat.2006.01.022.
[12] Duesterberg, C.K., Mylon, S.E., Waite, T.D., 2008. pH effects on iron-catalyzed oxidation using Fenton's reagent. Environ Sci Technol 42 (22), 8522–8527. https://doi.org/10.1021/es801720d.
[13] Fida, H., Zhang, G., Guo, S., Naeem, A., 2017. Heterogeneous Fenton degradation of organic dyes in batch and fixed bed using La-Fe montmorillonite as catalyst. J Colloid Interface Sci 490, 859–868. https://doi.org/10.1016/j.jcis.2016.11.085.
[14] Frisch, M., Trucks, G., Schlegel, H., Scuseria, G., Robb, M., Cheeseman, J., Scalmani, G., Barone, V., Petersson, G., Nakatsuji, H., 2016. Gaussian16. Gaussian, Inc, Wallingford, CT.
[15] Ghernaout, D., Elboughdiri, N., Ghareba, S., 2020. Fenton technology for wastewater treatment: dares and trends. Open Access Libr J 7 (1), 1–26. https://doi.org/10.4236/oalib.1106045.
[16] Giannakis, S., Liu, S., Carratala, A., Rtimi, S., Talebi Amiri, M., Bensimon, M., Pulgarin, C., 2017. Iron oxide-mediated semiconductor photocatalysis vs. heterogeneous photo-Fenton treatment of viruses in wastewater. Impact of the oxide particle size. J Hazard Mater 339, 223–231. https://doi.org/10.1016/j.jhazmat.2017.06.037.
[17] Guo, J., Wang, Y., Shang, Y., Yin, K., Li, Q., Gao, B., Li, Y., Duan, X., Xu, X., 2024. Fenton-like activity and pathway modulation via single-atom sites and pollutants comediates the electron transfer process. PNAS 121 (3), e2313387121. https://doi.org/10.1073/pnas.2313387121.
[18] Halladja, S., Ter Halle, A., Aguer, J.P., Boulkamh, A., Richard, C., 2007. Inhibition of humic substances mediated photooxygenation of furfuryl alcohol by 2,4,6-trimethylphenol. Evidence for reactivity of the phenol with humic triplet excited states. Environ Sci Technol 41 (17), 6066–6073. https://doi.org/10.1021/es070656t.
[19] Hameed, B.H., Lee, T.W., 2009. Degradation of malachite green in aqueous solution by Fenton process. J Hazard Mater 164 (2-3), 468–472. https://doi.org/10.1016/j.jhazmat.2008.08.018.
[20] Haydari, I., Aziz, K., Kaya, S., Dastan, T., Ouazzani, N., Mandi, L., Aziz, F., 2023. Green synthesis of reduced graphene oxide and their use on column adsorption of phenol from olive mill wastewater. Process Saf Environ Prot 170, 1079–1091. https://doi.org/10.1016/j.psep.2022.12.086.
[21] He, M.Q., Guo, X.R., Huang, J.Z., Shen, H.H., Zeng, Q., Wang, L.S., 2018. Mass production of tunable multicolor graphene quantum dots from an energy resource of coke by a one-step electrochemical exfoliation. Carbon 140, 508–520. https://doi.org/10.1016/j.carbon.2018.08.067.
[22] He, Y., Qin, H., Wang, Z., Wang, H., Zhu, Y., Zhou, C., Zeng, Y., Li, Y., Xu, P., Zeng, G., 2024. Fe-Mn oxycarbide anchored on N-doped carbon for enhanced Fenton-like catalysis: importance of high-valent metal-oxo species and singlet oxygen. Appl Catal, B 340, 123204. https://doi.org/10.1016/j.apcatb.2023.123204.
[23] Hoang, V.C., Dave, K., Gomes, V.G., 2019. Carbon quantum dot-based composites for energy storage and electrocatalysis: mechanism, applications and future prospects. Nano Energy 66, 104093. https://doi.org/10.1016/j.nanoen.2019.104093.
[24] Huang, X., Tian, Y.C., Li, A.M., Feng, Y.F., Li, D.W., 2023. Low-crystalline FeOx on carboxylic CNTs as high-performance Fenton-like catalysts: influence of crystallinity and carbon matrix. J Clean Prod 429, 139531. https://doi.org/10.1016/j.jclepro.2023.139531.
[25] Jaiswal, S., Kumar Gupta, G., Panchal, K., Mandeep, Shukla, P., 2020. Synthetic organic compounds from paper industry wastes: integrated biotechnological interventions. Front Bioeng Biotechnol 8, 592939. https://doi.org/10.3389/fbioe.2020.592939.
[26] Jiang, C., Pang, S., Ouyang, F., Ma, J., Jiang, J., 2010. A new insight into Fenton and Fenton-like processes for water treatment. J Hazard Mater 174 (1-3), 813–817. https://doi.org/10.1016/j.jhazmat.2009.09.125.
[27] Jiang, H., Dang, C., Liu, W., Wang, T., 2020. Radical attack and mineralization mechanisms on electrochemical oxidation of p-substituted phenols at boron-doped diamond anodes. Chemosphere 248, 126033. https://doi.org/10.1016/j.chemosphere.2020.126033.
[28] Jiang, Y., Ran, J., Mao, K., Yang, X., Zhong, L., Yang, C., Feng, X., Zhang, H., 2022. Recent progress in Fenton/Fenton-like reactions for the removal of antibiotics in aqueous environments. Ecotoxicol Environ Saf 236, 113464. https://doi.org/10.1016/j.ecoenv.2022.113464.
[29] Kasinathan, K., Samayanan, S., Marimuthu, K., Yim, J.H., 2022. Green synthesis of multicolour fluorescence carbon quantum dots from sugarcane waste: investigation of mercury (II) ion sensing, and bio-imaging applications. Appl Surf Sci 601, 154266. https://doi.org/10.1016/j.apsusc.2022.154266.
[30] Kumar, M.S., Yasoda, K.Y., Kumaresan, D., Kothurkar, N.K., Batabyal, S.K., 2018. TiO_2-carbon quantum dots (CQD) nanohybrid: enhanced photocatalytic activity. Mater Res Express 5 (7), 075502. https://doi.org/10.1088/2053-1591/aacbb9.
[31] Kurniawan, T.A., Sillanpää, M.E.T., Sillanpää, M., 2012. Nanoadsorbents for remediation of aquatic environment: local and practical solutions for global water pollution problems. Crit Rev Environ Sci Technol 42 (12), 1233–1295. https://doi.org/10.1080/10643389.2011.556553.
[32] Li, N., Liu, T.C., Xiao, S.Z., Chen, J.B., Xu, Y., Ji, R.C., Zhou, X.F., Zhang, Y.L., 2022. Iron cycle tuned by thiosulfate in Fenton reactions: kinetic modelling and mechanisms. Chem Eng J 431, 134252. https://doi.org/10.1016/j.cej.2021.134252.
[33] Li, X., Ge, F., Li, X., Zhou, X., Qian, J., Fu, G., Shi, L., Xu, Y., 2019. Rapid and large-scale production of carbon dots by salt-assisted electrochemical exfoliation of graphite rods. J Electroanal Chem 851, 113390. https://doi.org/10.1016/j.jelechem.2019.113390.
[34] Li, X., Zhao, Z., 2014. Facile ionic-liquid-assisted electrochemical synthesis of size-controlled carbon quantum dots by tuning applied voltages. RSC Adv 4 (101), 57615–57619. https://doi.org/10.1039/c4ra09274k.
[35] Li, Y.B., Liang, J.X., Li, J.D., Liao, L.Y., Guo, J.X., Jia, J.P., 2024. Tuning the carboxyl content of carbon quantum dots by an electrochemical exfoliation method to enhance Fenton-like reactions for contaminants removal in a wide pH range. J Environ Chem Eng 12 (2), 112008. https://doi.org/10.1016/j.jece.2024.112008.
[36] Lin, H., Ding, L., Zhang, B., Huang, J., 2018. Detection of nitrite based on fluorescent carbon dots by the hydrothermal method with folic acid. R Soc Open Sci 5 (5), 172149. https://doi.org/10.1098/rsos.172149.
[37] Liu, J.H., Li, X.Y., Chu, Y.Y., Yuan, L., Lv, R.L., Zhang, W.M., 2023. An autocatalytic Fe(III)/H_2O_2 Fenton-like process triggered by tetracycline: the overlooked effect of quinone intermediates. Chem Eng J 475, 146035 https://doi.org/ARTN14603510.1016/j.cej.2023.146035.
[38] Liu, Y., Yuan, Y., Wang, Y., Ngo, H.H., Wang, J., 2024. Research and application of active species based on high-valent iron for the degradation of pollutants: a critical review. Sci Total Environ 924, 171430. https://doi.org/10.1016/j.scitotenv.2024.171430.
[39] Lu, M.J., Lin, S.Y., Ma, X.L., Xu, Z.Z., Yang, H., Wang, M.F., Piao, J.X., Zhang, J.Q., Dong, P., Zhao, C.C., 2024. Enhanced mass transfer by 3D printing to promote the degradation of organic pollutants in electro-Fenton system. Chem Eng J 495, 153720. https://doi.org/10.1016/j.cej.2024.153720.
[40] Lu, T., 2024. A comprehensive electron wavefunction analysis toolbox for chemists, Multiwfn. J Chem Phys 161 (8). https://doi.org/10.1063/5.0216272.
[41] Lu, T., Chen, F., 2012. Multiwfn: a multifunctional wavefunction analyzer. J Comput Chem 33 (5), 580–592. https://doi.org/10.1002/jcc.22885.
[42] Lv, T., Suo, L., 2021. Water-in-salt widens the electrochemical stability window: thermodynamic and kinetic factors. Curr Opin Electrochem 29, 100818. https://doi.org/10.1016/j.coelec.2021.100818.
[43] Mao, G.Z., Gao, Y., Zhou, H.L., Jin, W.Q., 2022. Tuning of solvent evaporation to prepare PEBA membrane with high separation performance for the pervaporation of phenol aqueous solution. J Membr Sci 656, 120638. https://doi.org/10.1016/j.memsci.2022.120638.
[44] Ming, H., Ma, Z., Liu, Y., Pan, K., Yu, H., Wang, F., Kang, Z., 2012. Large scale electrochemical synthesis of high quality carbon nanodots and their photocatalytic property. Dalton Trans 41 (31), 9526–9531. https://doi.org/10.1039/c2dt30985h.
[45] Qin, Y., Song, F., Ai, Z., Zhang, P., Zhang, L., 2015. Protocatechuic acid promoted alachlor degradation in Fe(III)/H_2O_2 Fenton system. Environ Sci Technol 49 (13), 7948–7956. https://doi.org/10.1021/es506110w.
[46] Rasal, A.S., Yadav, S., Yadav, A., Kashale, A.A., Manjunatha, S.T., Altaee, A., Chang, J.Y., 2021. Carbon quantum dots for energy applications: a review. ACS Appl Nano Mater 4 (7), 6515–6541. https://doi.org/10.1021/acsanm.1c01372.
[47] Rocco, D., Moldoveanu, V.G., Feroci, M., Bortolami, M., Vetica, F., 2023. Electrochemical synthesis of carbon quantum dots. ChemElectroChem 10 (3), e202201104. https://doi.org/10.1002/celc.202201104.
[48] Shen, T., Tian, K., Cao, M., Li, L., Shi, F., Qu, J., Zheng, Q., Zhang, G., 2023. Application of nickel foam supported Cu–MnO_2 in microwave enhanced Fenton-like process for p-nitrophenol removal: degradation, synergy and mechanism insight. J Clean Prod 397, 136442. https://doi.org/10.1016/j.jclepro.2023.136442.
[49] Shen, X., Wang, Z., Guo, H., Lei, Z., Liu, Z., Wang, L., 2023. Solvent engineering of oxygen-enriched carbon dots for efficient electrochemical hydrogen peroxide production. Small 19 (43), e2303156. https://doi.org/10.1002/smll.202303156.
[50] Sun, H.Z., Wu, P.Y., 2018. Tuning the functional groups of carbon quantum dots in thin film nanocomposite membranes for nanofiltration. J Membr Sci 564, 394–403. https://doi.org/10.1016/j.memsci.2018.07.044.
[51] Vasilopoulou, M., Kim, H.P., Kim, B.S., Papadakis, M., Gavim, A.E.X., Macedo, A.G., da Silva, W.J., Schneider, F.K., Teridi, M.A.M., Coutsolelos, A.G., Yusoff, A.B., 2020. Efficient colloidal quantum dot light-emitting diodes operating in the second near-infrared biological window. Nat Photonics 14 (1), 50–56. https://doi.org/10.1038/s41566-019-0526-z.
[52] Wang, F.-X., Wang, C.-C., Du, X., Li, Y., Wang, F., Wang, P., 2022. Efficient removal of emerging organic contaminants via photo-Fenton process over micron-sized Fe-MOF sheet. Chem Eng J 429, 132495. https://doi.org/10.1016/j.cej.2021.132495.
[53] Wang, G., Huang, D., Cheng, M., Du, L., Chen, S., Zhou, W., Li, R., Li, S., Huang, H., Xu, W., Tang, L., 2024. The surface confinement of FeO assists in the generation of singlet oxygen and high-valent metal-oxo species for enhanced fenton-like catalysis. Small 20 (37), e2401970. https://doi.org/10.1002/smll.202401970.
[54] Wang, J., Zhang, L., He, Y., Ji, R., 2024. Biodegradation of phenolic pollutants and bioaugmentation strategies: a review of current knowledge and future

perspectives. J Hazard Mater 469, 133906. https://doi.org/10.1016/j.jhazmat.2024.133906.
[55] Wu, P.F., Zhou, C.L., Li, Y.P., Zhang, M.H., Tao, P.X., Liu, Q.L., Cui, W.Q., 2021. Flower-like FeOOH hybridized with carbon quantum dots for efficient photo-Fenton degradation of organic pollutants. Appl Surf Sci 540, 148362. https://doi.org/10.1016/j.apsusc.2020.148362.
[56] Xia, Q., Yao, Z., Zhang, D., Li, D., Zhang, Z., Jiang, Z., 2019. Rational synthesis of micronano dendritic ZVI@ Fe_3O_4 modified with carbon quantum dots and oxygen vacancies for accelerating Fenton-like oxidation. Sci Total Environ 671, 1056–1065. https://doi.org/10.1016/j.scitotenv.2019.03.435.
[57] Xiang, Y., Liu, H.L., Zhu, E.R.Y., Yang, K., Yuan, D.L., Jiao, T.F., Zhang, Q.R., Tang, S.F., 2022. Application of inorganic materials as heterogeneous cocatalyst in Fenton/Fenton-like processes for wastewater treatment. Sep Purif Technol 295, 121293. https://doi.org/10.1016/j.seppur.2022.121293.
[58] Xie, L.Q., Zhao, G.L., Jiang, X.Y., Yu, J.G., 2023. Rape seedling peel-derived biochar prepared by low-temperature vacuum pyrolysis method for adsorbing p-nitrophenol. Int J Environ Anal Chem 1–19. https://doi.org/10.1080/03067319.2022.2164492.
[59] Xing, M.Y., Xu, W.J., Dong, C.C., Bai, Y.C., Zeng, J.B., Zhou, Y., Zhang, J.L., Yin, Y. D., 2018. Metal Sulfides as excellent co-catalysts for H_2O_2 decomposition in advanced oxidation processes. Chem 4 (6), 1359–1372. https://doi.org/10.1016/j.chempr.2018.03.002.
[60] Yang, Y., Wang, Q., Li, G., Guo, W., Yang, Z., Liu, H., Deng, X., 2023. Cysteine-derived chiral carbon quantum dots: a fibrinolytic activity regulator for plasmin to target the human islet amyloid polypeptide for type 2 diabetes mellitus. ACS Appl Mater Interfaces 15 (2), 2617–2629. https://doi.org/10.1021/acsami.2c17975.
[61] Yu, B.Y., Kwak, S.Y., 2012. Carbon quantum dots embedded with mesoporous hematite nanospheres as efficient visible light-active photocatalysts. J Mater Chem 22 (17), 8345–8353. https://doi.org/10.1039/c2jm16931b.
[62] Zhang, C., Liu, L.W., Pan, Y.W., Qin, R., Wang, W., Zhou, M.H., Zhang, Y., 2025. Detection methodologies and mechanisms of reactive oxygen species generated in Fenton/Fenton-like processes. Sep Purif Technol 355, 129578 https://doi.org/ARTN12957810.1016/j.seppur.2024.129578.
[63] Zhang, M.-h, Dong, H., Zhao, L., Wang, D.-x, Meng, D., 2019. A review on Fenton process for organic wastewater treatment based on optimization perspective. Sci Total Environ 670, 110–121. https://doi.org/10.1016/j.scitotenv.2019.03.180.
[64] Zhang, R., Wang, X., Ali, A., Su, J., Wang, Z., Li, J., Liu, Y., 2022. Single-step removal of calcium, fluoride, and phenol from contaminated water by Aquabacterium sp. CZ3 via facultative anaerobic microbially induced calcium precipitation: kinetics, mechanism, and characterization. Bioresour Technol 361, 127707. https://doi.org/10.1016/j.biortech.2022.127707.
[65] Zhang, T., Wen, Y., Pan, Z., Kuwahara, Y., Mori, K., Yamashita, H., Zhao, Y., Qian, X., 2022. Overcoming acidic H_2O_2/Fe(II/III) redox-induced Low H_2O_2 utilization efficiency by carbon quantum dots Fenton-like catalysis. Environ Sci Technol 56 (4), 2617–2625. https://doi.org/10.1021/acs.est.1c06276.
[66] Zhou, H., Zhang, H., He, Y., Huang, B., Zhou, C., Yao, G., Lai, B., 2021. Critical review of reductant-enhanced peroxide activation processes: trade-off between accelerated Fe^{3+}/Fe^{2+} cycle and quenching reactions. Appl Catal B 286, 119900. https://doi.org/10.1016/j.apcatb.2021.119900.